JOURNAL OF APPLIED ELECTROCHEMISTRY 14 (1984) 277–284

A feasibility study of mercury deposition in a lead fluidized bed electrode

M. FLEISCHMANN

Department of Chemistry, The University, Southampton SO9 5NH, UK

G. H. KELSALL

Department of Mineral Resources Engineering, Imperial College, London SW7 2BP, UK

Received 30 June 1983, revised 10 October, 1983

Following previous work on the recovery of copper from very dilute solutions using a copper fluidized bed electrode, the behaviour of a lead fluidized bed electrode (FBE) is described, for the recovery of mercury from chloride solutions, as typified by chlor-alkali plant effluent.

Injection of known quantities of Hg(II) into the FBE catholyte and integration of the current vs time response followed by chemical analysis, allowed mean current efficiencies for mercury deposition to be determined as a function of : feeder electrode potential, Hg(II) concentration, flow rate, bed depth, particle size range, and reservoir volume. By judicious choice of these experimental variables, particularly by limiting bed depths to ~ 20 mm, (potentiostatic) current efficiencies for Hg(II) deposition of 99% could be achieved.

Nomenclature

a	cross sectional area of FBE cell (1.26×10^{-3} m^2)	I	current density ($A\,m^{-2}$)
A	area per unit volume of FBE electrode (m^{-1})	L	static bed length (mm)
$c(x)$	concentration at distance x from feeder electrode ($mol\,m^{-3}$)	t	time (s)
c_0	inlet concentration ($mol\,m^{-3}$)	T	catholyte temperature (K)
c_{XL}	outlet concentration ($mol\,m^{-3}$)	u	electrolyte superficial linear velocity ($mm\,s^{-1}$)
D	diffusion coefficient ($m^2\,s^{-1}$)	V	electrolyte volume (m^3)
		XL	expanded bed length (mm)
		δ	diffusion layer thickness (m)
		λ	characteristic length ($\delta u/DA$) (m)
		ρ	(lead) density ($11.4 \times 10^6\,g\,m^{-3}$)

1. Introduction

A major source of mercury-containing effluent has traditionally been the chlor-alkali industry [1, 2], although other sources such as catalyst streams of mercury-containing sulphuric acid, for example, from the production of α-anthraquinone disulphonic acid [3], may also present significant environmental hazards. Conventional mercury recovery routes involve chemical precipitation, as sulphide [4, 5] or thiosulphate [3], ion-exchange [6], or cementation, using a copper-coated nickel [7] or 'base metal' [8] fluidized bed. Other routes involve the use of hypochlorite [6, 9, 10] to produce soluble Hg(II), either from insoluble mercury species or from mercury metal, which may then be returned to the issuing chlor-alkali cell, in which recovery is achieved by deposition at the mercury cathode.

Following the successful removal of copper from dilute solutions using a copper fluidized bed electrode (FBE) [11–13], a lead particle FBE was constructed to test the feasibility of tackling mercury effluent problems by electrodeposition on such high surface area electrodes. In preliminary work using a

0021–891X/84 $03.00 + .12

non-amalgamating nickel rotating disc electrode to study the kinetics of mercury deposition from chloride solutions, elemental mercury droplets lost from the electrode caused calomel precipitation on the bottom of the cell by the reaction:

$$Hg_{(l)} + Hg^{2+} + 2Cl^- \rightarrow Hg_2Cl_{2(s)} \quad (1)$$

so removing electroactive Hg(II) species from the solution. To minimize this effect in the FBE, lead was chosen as the electrode material, since the phase diagram of the Pb–Hg system [14] indicates that at ambient temperatures, alloys with > 69 atomic % Pb are solid and single phase. However, this property is of benefit only if the rate of Hg deposition is sufficiently low to prevent a liquid phase forming on the surface of the electrode particles, i.e. if the rate of diffusion of lead through the amalgam phase to the surface is faster than the rate of Hg deposition; this condition can be satisfied using fluidized bed electrodes.

In the absence of depositable solution species such as Fe(II), the high hydrogen overpotential on lead (depending on the composition of the surface amalgam) is expected to be an additional advantage, in providing a large working potential range within the FBE.

Since this reported work was completed [15], van der Heiden *et al.* [16] have described the industrial use of a copper FBE for the treatment of a chlor-alkali effluent containing 1–5 ppm ionic and metallic mercury species in 4.5 mol dm^{-3} chloride solutions at pH 2–3. The 1.2 m deep cylindrical geometry cell, installed at Akzo Zout Chemie's Henglo plant in the Netherlands reduced the mercury level to < 100 ppb. Mercury recovery/copper particle electrode regeneration was achieved by distillation of the amalgam.

2. Experimental details

The 40 mm diameter FBE cell used was essentially that described previously [13, 15], except that the Luggin capillary probe for the saturated calomel electrode (SCE) was positioned below rather than above the bed, as shown in Fig. 1. In this configuration it is less likely that any portion of the bed can adopt a potential leading to dissolution of lead, accompanied by mercury deposition. A glass reservoir normally holding 2 dm^3 of 0.5 mol dm^{-3} NaCl (analytical grade) supporting electrolyte was used in the flow circuit. The remaining equipment and instrumentation used has also been described previously [14, 16].

The feeder electrode was a nickel gauze electroplated with lead from a solution containing: 0.4 dm^3 $Pb(BF_4)_2$ solution, s.g. 1.73 (Hoechst Chemicals), 0.5 g gelatine in a little hot water, 0.1 g resorcinol dissolved in a little methanol, and made up to 1 dm^3 with deionized water. After being sieved into the appropriate size ranges, the lead particles (BDH Ltd.) were cleaned in dilute aqueous HNO_3 and washed in deionized water prior to use. After loading the bed into the cell, pre-electrolysis was carried out until the cell current was less than 1 mA. Low flow rates were used at this stage so that the bed remained packed and the surface chloride, formed on immersion of the lead in the neutral 0.5 mol dm^{-3} NaCl electrolyte, could be reduced. The particles became progressively brighter as this process occurred, and once reduced, the electrode remained active even at high bed expansions. The pre-electrolysis also reduced any oxygen remaining in the electrolyte after deoxygenation by nitrogen bubbling, and any $PbCl_2$ dispersed in the solution as the bed was loaded.

A known volume of a standard aqueous solution of $HgCl_2$, calculated to produce the required concentration when thoroughly mixed with the catholyte, was injected by hypodermic syringe through a serum cap into the electrolyte reservoir. This had to be carried out with polarization of the bed at the desired feeder potential to prevent cementation with the formation of $PbCl_2$, so precluding thorough catholyte mixing by recirculation prior to cell operation. The response in cell current with time was monitored on a Y–t recorder, and integrated using a Gated Integrator (Hi-Tek Instruments Ltd).

Samples of the catholyte were analysed for Hg(II) on an atomic absorption spectrophotometer (Varian AA5), so that with the integrated current vs time data, mean current efficiencies could be determined. This procedure was carried out as a function of flow rate, feeder electrode potential, particle size range, Hg(II) concentration and electrolyte volume.

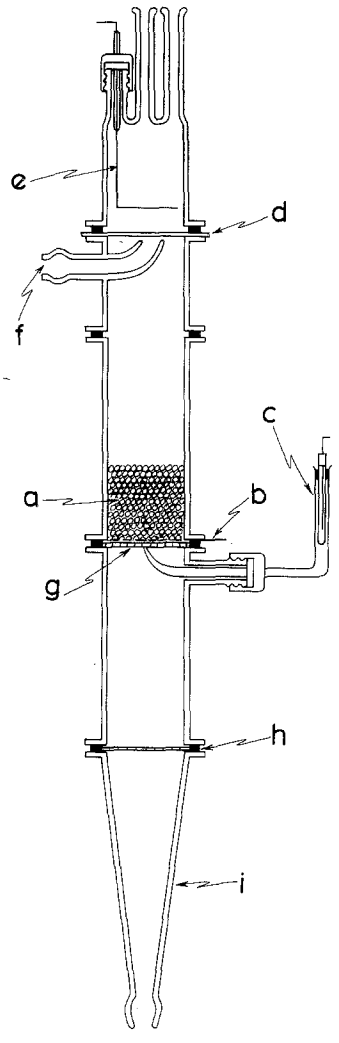

Fig. 1. Fluidized bed electrode cell. a is fluidized bed of lead particles, b is lead-plated nickel gauze feeder electrode, c is saturated calomel reference electrode, d is ion-exchange membrane, e is platinum anode, f is catholyte outlet, g is porous polythene distributor, h is 'O' ring seal and i is diffuser.

Difficulties were experienced with the bed agglomerating, particularly during the pre-electrolysis when it was known that $PbCl_2$ concentration formed and subsequently to be reduced, was relatively high. This difficulty was minimized by using the 500–600 μm particle size range.

3. Results and discussion

Prior to using the FBE of lead particles, the behaviour of a lead wire electrode (analytical grade, BDH Ltd) in various chloride media was studied to determine the working potential range for mercury deposition, tolerable in the bed. A typical cyclic voltammogram obtained is shown in Fig. 2a. The three important features are:

(a) a peak at -0.2 V (SCE) resulting from $PbCl_2$ formation, due to a dissolution/precipitation mechanism

$$PbCl_2 + 2e \rightleftharpoons Pb + 2Cl^- \qquad E^\ominus = -0.268 \text{ V vs SHE} \tag{2}$$

(b) a peak at -0.7 V (SCE) and a mass transport controlled current plateau region from -1.0 to -1.9 V (SCE) due to $PbCl_2$ reduction

(c) an increase in current at -1.9 V (SCE) due to hydrogen evolution

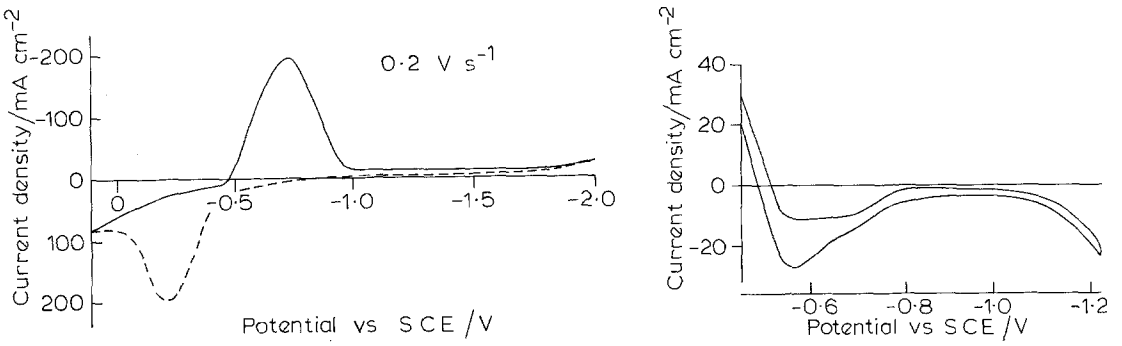

Fig. 2 (a) Cyclic voltammogram of Pb in 0.5 mol dm^{-3} NaCl, (b) Cyclic voltammogram for a FBE of 200 g 710–850 μm Pb particles, L = 25 mm, XL = 36 mm, in 0.5 mol dm^{-3} NaCl flowing at 67 mm s^{-1}.

The large separation (~ 0.5 V) of peaks a and b may be due to the irreversibility of the phase growth process and/or reaction of the lead chloride to form oxychloride which will be more difficult to reduce than the chloride. Addition of 10^{-4} mol dm^{-3} $HgCl_2$ to the 0.5 mol dm^{-3} NaCl caused little apparent change to the voltammogram, with the Hg(II) providing a constant (mass transport limited) background current due to its reduction by the reaction

$$HgCl_4^{2-} + 2e \rightleftharpoons Hg + 4Cl^- \qquad E^{\ominus} = +0.403 \text{ V vs SHE} \tag{3}$$

However, addition of 10^{-3} mol dm^{-3} $HgCl_2$ reduced the peak separation to ~ 80 mV, presumably due to the effect of the formation of a liquid surface amalgam phase on the kinetics of the Pb dissolution/deposition reaction.

The voltage span of the cathodic current range, prior to the onset of hydrogen evolution, indicated that a working potential range of ~ 1 V would be available in a lead FBE (depending on pH, Pb(II) interfacial concentration, and the presence of impurities) for the mass transport controlled reduction of Hg(II). The absence of complicating effects due to the chemical dissociation of complex species [2] such as $HgCl_x^{(x-2)-}$, was confirmed using a rotating disc electrode, the details of which have been described previously [15].

Fig. 2b shows a typical cyclic polarization curve for a lead particle FBE in 0.5 mol dm^{-3} NaCl. The anodic current at − 0.5 V (SCE) is due to the onset of lead dissolution leading to the formation of $PbCl_2$, and the cathodic peak at − 0.6 V is due to $PbCl_2$ reduction. The levelling out of the current at − 0.6 to − 0.7 V may be due to trace impurities in the lead (which was not analytical grade) or may be a double layer charging effect. The plateau region from − 0.8 to − 1.05 V (SCE) is due to the

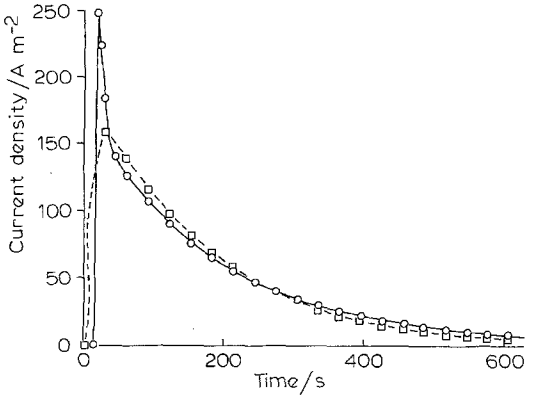

Fig. 3. Current–time responses of a 100 g, L = 13 mm 600–710 μm Pb FBE after injection of 2 × 10^{-4} mol Hg(II) to 2 dm^3 of 0.5 mol dm^{-3}. − 1.0 V vs SCE feeder electrode potential, T = 303 K. (——) u = 33 mm s^{-1}, XL = 15 mm (– – –) u = 53 mm s^{-1}, XL = 17 mm.

mass transport controlled reduction of $PbCl_2$, while the increase in current at < 1.1 V is due to hydrogen evolution. Evidently high potentials, sufficient to cause visible hydrogen evolution, were generated at the top of the bed, while the feeder electrode was still at -1.05 V (SCE) (c.f. Fig. 2a).

Fig. 3 shows typical current vs time response curves following the injection of a standard $HgCl_2$ solution. The peak current was taken as a measure of the expected steady state current had complete mixing taken place. By electronic integration of the I/t curve and electrolyte analysis by atomic absorption spectrophotometry, a mean current efficiency for the depletion of the Hg(II) species could be determined. Typical values for 100 g Pb particles ($L = 13$ mm) were 99% for the 600–710 and 710–850 μm particle size ranges, and the Hg(II) concentrations after 20 minutes depletion from an initial 20 ppm (10^{-4} mol dm^{-3}) in a 2 dm^3 electrolyte volume, were often below the detection limit for atomic absorption spectrophotometry (< 2 ppb), i.e. a concentration reduction of more than four orders of magnitude. The efficiency appeared to be largely independent of feeder electrode potential over the range -0.6 to -1.0 V (SCE), in the mass transport controlled $PbCl_2$ reduction region of the polarization curve (Fig. 2b). For the 500–600 μm and 850–1000 μm particle size ranges, lower current efficiency values of $\sim 95\%$ and $\sim 85\%$ respectively were obtained. This decrease was probably due to low frequency oscillations (~ 1 Hz), which occurred with certain potential/flow rate combinations, due to the difficulties of controlling an electrode having the characteristics of an R–C delay line.

Doubling the bed weight/height to 200 g/$L = 25$ mm was found to reduce the current efficiency to 50–65% for -0.7 to -0.8 V vs SCE feeder electrode potentials, and 34% at -0.95 V SCE for the 710–850 μm particle size range at a fluid velocity of 53 mm s^{-1} ($XL = 28$ mm). The contraction in working potential range with increasing bed depth can be explained in terms of the changed potential profiles, generating a sufficiently high overpotential at the top of the bed to cause hydrogen evolution, even at modest feeder electrode potentials.

The peak currents obtained for various flow rates and particle size ranges, are shown in Fig. 4. Incomplete mixing of the concentrated Hg(II) solution injected into the electrolyte reservoir prior to cell operation, precludes their quantiative interpretation. However, the deviation from the true steady state current densities is unlikely to be very great, as can be seen from the small deviation from the expected exponential decay of the current vs time curves shown in Fig. 6. The values of the (membrane) current densities therefore, can be taken to demonstrate a scale-up factor of 100–300 compared with a conventional plate electrode. This is broadly in agreement with the results of Tennakoon *et al.* [11] for copper deposition in a copper FBE operating wholly under diffusion/depletion control.

The effect of concentration of Hg(II) over the range 2–25 ppm, is shown in Fig. 5, the current densities again being taken from the peak values of the current vs time curves. The relationship appears to be linear, confirming a mass transport controlled reaction. The high values of current density for 20 and 25 ppm Hg(II), can be explained in terms of slightly lower current efficiencies due to some hydrogen evolution.

The dependence of the current vs time curves on the reservoir volume, for the depletion of an

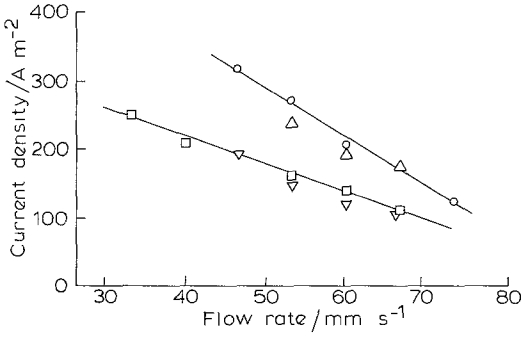

Fig. 4. Peak current densities (*ip*) as a function of flow rate of 0.5 mol dm^{-3} NaCl $-$ 10^{-4} mol dm^{-3} $HgCl_2$ through a 100 g, $L = 13$ mm Pb FBE of 500–600 μm (▽), 600–710 μm (▣), 710–850 μm (⊙) and 850–1000 μm (△) particles, with -1.0 V vs SCE feeder electrode potential.

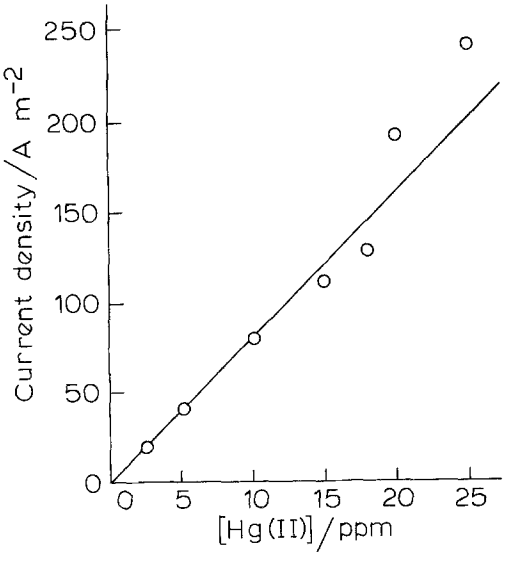

Fig. 5. Effect of Hg(II) concentration on FBE current density. 100 g, L = 13 mm 500–600 μm Pb particles in 0.5 mol dm^{-3} NaCl – x ppm Hg(II), u = 47 mm s^{-1}, XL = 17 mm, T = 293 K, – 0.6 V vs SCE feeder electrode potential.

electroactive species, with the FBE operating wholly under mass transport control, may be calculated from a model which assumes plug flow, i.e. no radial or axial mixing of the electrolyte [12, 17].

Under these conditions, the steady state concentration profile in the bed is given by

$$c(x) = c_0 \exp(-x/\lambda) \tag{4}$$

where the characteristic length, λ is given by

$$\lambda = \delta u/DA \tag{5}$$

making the correction to the original term [17], as suggested by Walker and Wragg [18].

The current density for the cell (I) is obtained from the mass balance for the electrode using Equation 1 to give the concentration at the top of the electrode (XL)

$$I = nFc_0u[1 - \exp(-XL/\lambda)] \tag{6}$$

If the electrolyte volume is V, then a mass balance for the reservoir gives

$$V \cdot \frac{dc_0}{dt} = au(c_{XL} - c_0) \tag{7}$$

where a is the cell cross sectional area, u is the electrolyte superficial linear velocity, and c_{XL}, c_0 are the concentrations of electroactive species at the outlet and inlet of the cell respectively.

Substituting from Equation 4 gives

$$V \cdot \frac{dc_0}{dt} = auc_0[\exp(-XL/\lambda) - 1] \tag{8}$$

Integration of Equation 8 with the initial condition $t = 0$, $c_0 = c_0^0$, gives

$$c_0 = c_0^0 \exp\left\{-\frac{aut}{V}[1 - \exp(-XL/\lambda)]\right\} \tag{9}$$

Substituting Equation 9 into Equation 6 gives

$$I = nFu\, c_0^0[1 - \exp(-XL/\lambda)] \exp\left\{-\frac{aut}{V}[1 - \exp(-XL/\lambda)]\right\} \tag{10}$$

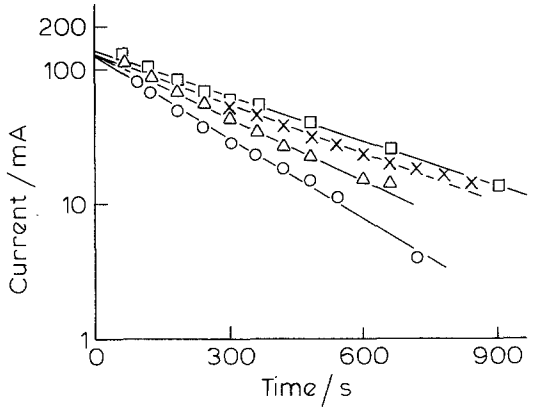

Fig. 6. Effect of electrolyte volume on the current decay during the recycle electrolysis of 0.5 mol dm^{-3} NaCl – 10 ppm Hg(II) through a 100 g, L = 13 mm 500–600 μm Pb particle FBE. u = 47 mm s^{-1}, XL = 17 mm, – 0.6 V vs SCE feeder electrode potential. ⊙ 2 dm^3, △ 3 dm^3, × 4 dm^3, ⊡ 5 dm^3 electrolyte volume.

Walker and Wragg [18] derived a similar equation more rigorously, and subsequently showed [19] that a plug flow approximation gives reasonable agreement between their experimental data and the theoretical model.

Fig. 6 shows current vs time curves for the depletion of 10 ppm Hg(II) during recycle electrolysis of different electrolyte volumes. While the lack of thorough mixing of the concentrated Hg(II)-containing solution into the base electrolyte prior to cell operation precludes a quantitative analysis, a rough fit with Equation 10 is obtained. With a mean diameter, $\bar{d}$, of 5.5 × 10^{-4} m, for particles in the 500–600 μm range the area of the fluidized bed electrode is 0.096 m^2 and the total area (including the gauze feeder electrode) is 0.097 m^2. With this value, the mass transport rate coefficient, k_m, derived from the initial currents in Fig. 6 is 1.4 × 10^{-4} m s^{-1}. This high value at the relatively low flow rates is due to turbulence within the bed. Substitution of k_m and the other data for Fig. 6 into Equation 10 gives

$$\ln I = 4.53 - \frac{0.012}{V} \cdot t \tag{11}$$

The slopes of the four lines in Fig. 6 agree with the value $-(0.012/V)$, to within + 5, – 10 and – 24% for 5, 4, 3 and 2 dm^3 of electrolyte respectively. As the t = 0 value of the cross-sectional current density I = 103 A m^{-2} is 11% higher than the predicted value of 92.6 A m^{-2} (due to the mode of injection of Hg(II) species) the expected error in the slope is greatest for the smallest electrolyte volume.

The mercury recovery/lead particle regeneration processes have not been studied but clearly electrochemical recoveries are precluded by the respective electrode potentials. A thermal route is therefore necessary. However, as the boiling point of Hg (630 K) is inconveniently greater than the melting point of Pb (600 K), a low pressure distillation would be required; this inevitably would be slow, though less energy intensive than melting of the lead during Hg distillation with subsequently reshotting.

Clearly the practical significance of any Hg metal loss from the electrode surface needs to be assessed. Electrode materials such as the Cu used by Akzo [16] have the advantage of remaining solid well above the boiling point of Hg, so allowing distillation at rates limited by solid state diffusion of Hg from the core to the surface of the electrode particle. However, as the compositional range over which Cu–Hg alloys are solid is more restricted than that of Pb–Hg [14], more frequent 'unloading' of the Hg from the bed would be required, if liquid Hg is to be avoided under FBE operation conditions. This constraint also limits the (particle) current density Hg deposition rate to less than the rate of diffusion of Hg into the particle core.

4. Conclusions

The experimental results establish that a lead shot FBE can be used for the removal of Hg(II) species from aqueous chloride solutions, and that with careful choice of operating conditions, typical current

efficiencies of 99% can be achieved, leaving 2 ppb Hg(II) in solution. The scale-up in (cross-sectional) current density, compared to a conventional plate electrode, was found to be more than two orders of magnitude, in agreement with the work of Tennakoon [11, 12] on a copper-depositing FBE. As the current efficiency for Hg deposition falls with increasing bed depth, in a practical device the dimension in the direction of current flow would be limited to ~ 20 mm so that a 'flow by' configuration would be used.

References

[1] B. Commoner, *Chem. Br.*, 8 (1972) 52.
[2] R. Caban and T. W. Chapman, *AIChE J.* **18** (1972) 892.
[3] Sumitomo Chemical Co. Ltd., German Patent 2 321 196 (1973).
[4] For example *Chem. Abs.* **81** 82126e.
[5] *ibid.* **81** 111188j.
[6] W. C. Gardiner and F. Munoz, *Chem. Eng.* 78 (1971) 57.
[7] D. J. Flood and C. J. Kraynik, *Chem. Abs.* 83 (1973) 65287g.
[8] P. E. Waltrich, US Patent 3 704 875 (1972).
[9] E. Wygasch and G. Weiss, US Patent 3 755 110 (1973).
[10] BP Chemicals Ltd., British Patent 1 336 084 (1973).
[11] C. L. K. Tennakoon, PhD thesis, Southampton University (1971).
[12] M. Fleischmann, J. W. Oldfield and L. Tennakoon, *J. Appl. Electrochem.* **1** (1971) 103.
[13] M. Fleischmann and G. H. Kelsall, *ibid.* **14** (1984) 269.
[14] M. Hansen, 'Constitution of Binary Alloys', McGraw-Hill, London (1958).
[15] G. H. Kelsall, PhD Thesis, Southampton University (1975).
[16] G. van der Heiden, C. M. S. Raats and H. F. Boon, *Chem. Ind.* **13** (1978) 465.
[17] M. Fleischmann and J. W. Oldfield, *J. Electroanal. Chem.* **29** (1971) 211.
[18] A. T. S. Walker and A. A. Wragg, *Electrochim. Acta* **22** (1977) 1129.
[19] *Idem, Chem. Eng. Sci.* **35** (1980) 405.